This article has been accepted for publication in a future issue of this journal, but has not been fully edited. Content may change prior to final publication. Citation information: DOI 10.1109/TMECH.2018.2790922, IEEE/ASME Transactions on Mechatronics

A Modal Expansion Method for Displacement and Strain Field Reconstruction of a Thin-wall Component during Machining

Man Yu[1], Jiajie Guo[1*], *IEEE/ASME Member*, and Kok-Meng Lee[1,2*], *Fellow, IEEE/ASME*

***Abstract*— Machining complex thin-wall components (such as compressor disks and casings in aircraft engines) has been a challenging task because workpiece deformations and vibrations not only compromise the surface integrity but also induce residual stresses in the final products. This paper offers a physics-based method that accounts for the damping effects and external loads for reconstructing the dynamic displacement and strain fields of a thin-wall workpiece in real-time with non-contact displacement measurements during machining. Given that part dynamic behaviors can be characterized by superposition of mode shapes, the time-varying displacement and strain fields are reconstructed with modal coefficients that are updated in real time using in situ measurements. The reconstruction method has been numerically verified with finite element analyses with the sensor locations optimized using a genetic algorithm; both static and dynamic field reconstructions are analyzed. Tradeoffs between the number of sensors and the reconstruction efficiency in terms of computation time and error are discussed. The method has been evaluated experimentally on a lathe machine testbed, where the dynamics of the distributed physical fields have been successfully captured and analyzed, demonstrating its practicality as a real-time tool for continuously monitoring the displacement and strain distributions across a disk workpiece during machining.**

***Index Terms*— field reconstruction, displacement and strain, thin elastic plate, process monitoring, dynamics, intelligent sensing**

NOMENCLATURE

Capitalized symbols

E	Elastic modulus	F	External force
P	General physical field	R	Normalized radius
K	Number of mode shapes	N	Number of sensors
W	Normalized displacement		

Lowercase symbols

a	Outer radius	b	Inner radius
e	Normalized strain	h	Thickness
n	Nodal radius	m	Nodal circle
t	Time	r	Radius
v	Tool feedrate	w	Displacement

Greek symbols

Ω	Rotational speed	Θ	Normalized angle
Φ	Mode shape	θ	Angle
α	Modal coefficient	ε	Strains
τ	Normalized time	ρ	Density
υ	Poisson ratio		

This research was supported by the National Basic Research Program of China (973 Program, Grant No. 2013CB035803), National Nature Science Foundation of China under Grant 51505164, and the U.S. National Science Foundation (Grant CMMI-1662700).

Man Yu and Jiajie Guo are with the State Key Lab. of Dig. Manuf. and Equip. Tech. (SKL-DMET), and Sch. of Mech. Sci. and Eng. at Huazhong Univ. of Sci. and Tech. (HUST), Wuhan, Hubei, 430074, P. R. China. Kok-Meng Lee is with the Woodruff Sch. of Mech. Eng. at Georgia Inst. of Tech., Atlanta, GA 30332-0405 USA, and Distinguished Professor of the SKL-DMET at HUST.
**Corresponding authors*: Jiajie Guo (jiajie.guo@hust.edu.cn) and Kok-Meng Lee (kokmeng.lee@me.gatech.edu).

I. INTRODUCTION

With increasing demands for products with high strength to weight ratio, thin-wall component machining has become common in aviation industries. A good understanding of the stress and deformation caused by the vibration and the cutting force between the machine tool and the component is an essential prerequisite for the machining of the thin shell parts. Deformations are spatially distributed across the thin-wall workpiece during machining; the main causes of distortions are vibrations under cutting forces and machining-induced surface residual stresses that are among the critical problems [1]. Displacement and strain distributions in a thin-wall component due to external loads (such as cutting and clamping) play an important role in assessing residual stresses and surface integrity of a machined product. As a main feature in intelligent manufacturing equipment [2], field sensing is essential to online compensation with autonomous process parameter updating. Motivated by the interests to improve "first time yield" and manufacture components at a faster rate while minimizing scraps, this paper presents a new non-contact approach to characterize the dynamic displacement and strain fields in real time for continuously monitoring their distributions across a disk workpiece during machining.

Machine vision with various advanced sensing principles has been used to capture field-based information. The shape and deformation of a vibrating structure can be captured with 3D digital image correlation methods [3]. With the known force-deflection characteristics, a force sensor has been developed by observing displacements of the selected points in the compliant mechanism with a CCD camera [4]. Out-of-plane deformations of a specimen were captured in real time via full-field shadow moiré images to study how residual strains were built up in an epoxy molding compound during manufacturing [5]. Employing piezospectroscopic effects, where spectral emissions of photo-luminescent materials are sensitive to the strains or stresses, a portable system has been

This article has been accepted for publication in a future issue of this journal, but has not been fully edited. Content may change prior to final publication. Citation information: DOI 10.1109/TMECH.2018.2790922, IEEE/ASME Transactions on Mechatronics

developed for non-contact in-situ stress sensing [6]. An alternative to optic-based imaging methods (where the performance effectiveness depends on environmental conditions during machining) is to reconstruct physical fields numerically with discrete measurements. Intelligent robotics has been employed to collect field data for health monitoring of civil infrastructures [7]; such as a wall-climbing robot capable of impact-echo acoustic inspection for plate-like structures [8]. Typical field reconstruction methods numerically solve a boundary value problem (BVP) formulated with appropriate governing equations and boundary conditions interpolated from measured nodal information in the region of interests. The curvature-based beam model was employed to predict and control a soft robot which continuous deformations are numerically obtained by the shooting method [9]. The confluence algorithm was applied for constructing dynamic displacements of a rectangular plate using experimental measurements and a numerical model [10]. Finite element analysis (FEA) is one of the most common approaches to solve BVPs for predicting distributed dynamic responses with prescribed accuracy. However, most numerical methods for solving BVPs usually involve iterations at the expense of relatively long computational time thus not practical for real time applications. Combining FEA with statistical analysis, the time for simulating workpiece deflection under machining has been reduced from weeks to hours [11], but still it is too time costly for online computations.

The modal expansion technique that assumes displacements of a deformation or vibration as a linear combination of shape functions has been developed to improve computational efficiency. The displacement field of a wing-like plate was obtained with mode shapes and strain measurements for control applications and health monitoring [12]. Since mode shapes can be obtained in advance, a displacement field is reconstructed by evaluating each modal coefficient with an approximation of locally measured strains through a linear regression. Formulated using the variation principle to derive a displacement-strain relation, the three-dimensional (3D) deformed shape of a composite stiffened panel under a mechanical/thermal load was reconstructed in real time using an inverse-FEA with in-situ surface strain measurements [13], where the least-square regression was used to fit the calculated strains in FEA with measurements [14]. Given the differential relations between displacements and strains/curvatures, the bending of a beam was estimated by strain measurements [15], and the large deformations of a beam were calculated with the curvatures [9, 16]. The 3D deflected shape of a needle was predicted with local axial-strains measured by an array of Fiber Bragg Grating sensors [17]. Strain sensing was employed as a cost-effective method to reconstruct deformations in structural health monitoring [18, 19]. With the displacement field obtained from strain data using the above shape sensing methods, the process can be reversed through a spatial differentiation of the displacements to reconstruct the strain fields. The global dynamic strains in a wind turbine was extracted in a photogrammetric approach where motions of optical targets along the vibrating blades were tracked by high speed cameras, while the reconstruction accuracy depended on numerous tracking points covering the whole structures [20]. Besides, other physical quantities can also be obtained from displacement or strain data, such as stresses [21] and forces [4, 22], as long as their constitutive relations are known for a given mechanism. Though efficient for real-time reconstruction, the above shape sensing methods generally rely on strain sensors attached on the measured surfaces of the targeted structures. For material removal applications particularly rotating disks in aircraft engines and structural components in airframes, where workpiece parameters (inertia, damping and stiffness) are time varying, it is desired to develop a non-contact method for robust field sensing during machining.

To avoid difficulties encountered in direct strain sensing, this paper tales advantages of the non-contact eddy-current displacement sensing to reconstruct both the displacement and strain fields of a thin-wall compressor disk under lathe turning. Eddy-current displacement sensing has been found to be robust under machining conditions [23] and implemented for monitoring the spindle status of a computer numerically controlled (CNC) end milling machine [24]. Moreover, eddy-current dampers (ECD) have been developed to suppress beam-like structure vibrations [25, 26] providing a relatively large stability margin for tuning process parameters involved in machining thin-wall components. As compared to shape sensing with strain measurements, the method introduced here captures strain field dynamics with displacement data using a similar approach for displacement field reconstruction in [27]. To account for the geometrical changes due to material removal during machining, the mode shapes were numerically calculated and normalized by the plate thickness [23] for multiple cuts, and the mode-shapes of a stepped plate during one cut were investigated in [28]. In this paper, the calculated mode-shapes are stored in an offline database for real-time reconstruction during machining. The remainder of this paper offers the following:

- A general method that reconstructs both the displacement and strain fields from the same measured displacement data is formulated for real time applications where the dynamics of a thin-wall component can be characterized by a linear superposition of mode shapes obtainable offline. The formulation, along with the reconstruction algorithm, is numerically illustrated with FEA that simulates the "measured fields" as a basis for verification. Both static and dynamic field reconstructions are analyzed. As will be demonstrated with a thin-wall part machining experiment, the modal expansion method accounts for the damping effects and external loads in the reconstruction.
- In theory, the number of mode shapes for a distributed-parameter system could be infinite. However, in most of cases, only a finite set of vibration modes plays the leading role. The dominant vibration modes are identified in an impulse test. For numerically illustrating the mode shapes and investigating its effects on the reconstruction, all the detected vibration mode-shapes are calculated, and the tradeoffs between the number of mode-shapes and the computation efficiency/error are demonstrated where higher order modes are intentionally included in the simulation. For comparing with published results in [27] and [29], the sensing locations are optimized using a genetic algorithm for reconstruction with two mode-shapes of the lowest orders.

This article has been accepted for publication in a future issue of this journal, but has not been fully edited. Content may change prior to final publication. Citation information: DOI 10.1109/TMECH.2018.2790922, IEEE/ASME Transactions on Mechatronics

– Experimental results obtained on a machining testbed with the optimized sensing locations are presented; both rotating and non-rotating dynamic responses are considered. These results experimentally validate the method by comparing the reconstructed fields with three independent types of measurements; the laser and eddy-current displacement sensors, and strain gauges.

To the best of our knowledge, the experimental results presented here are among the first quantitative data reported on reconstructed strains during machining of a thin-wall workpiece. Apart from providing a guideline for designing ECD to minimize vibration, the reconstructed fields potentially offer essential information for online compensation with autonomous updating of process parameters.

II. FORMULATION OF FIELD RECONSTRUCTION

Figure 1 shows two examples of circular thin-wall (thickness h) components modeled in cylindrical coordinates $[\mathbf{e}_r\ \mathbf{e}_\theta\ \mathbf{e}_z]$, where the referenced mid-surfaces are spanned by $\mathbf{e}_r$ and $\mathbf{e}_\theta$ axes, and $\mathbf{e}_z$ is aligned with the revolution axis. Figures 1(a, b) illustrate an annular plate model where the radial dimension of the mid-surface is given by $b \le r \le a$; and the location of a plate element is described in terms of (r, θ). For a cylindrical shell ($r = a$) in Figs. 1(c, d), its element is located by the coordinates (z, θ). The constraints can be imposed on either one or both boundaries of the components; and the elements are subjected to plane strain states. As the thickness h which may be a non-uniform function of the element location is very small compared to its radius ($h << a$), the thin-wall component can be represented by its mid-surface, and has the smallest stiffness in the normal direction of its mid-surface. Thus, the deformation of the component is dominant by the out-of-surface displacement $w(t, r, \theta)$ for the plate model or $w(t, z, \theta)$ for the shell model. The interest here is to reconstruct the continuous distributions of the out-of-plane displacement field and normal/shear strains by superimposing the corresponding mode shapes, where the time-varying coefficients are determined by a finite set of local discrete measurements. The following formulation assumes that the material property is linear elastic and homogeneous across the component; and the shear deformations are neglected across the small thickness. The strain fields $\boldsymbol{\varepsilon} = [\varepsilon_{11}, \varepsilon_{22}, \varepsilon_{12}]^T$ are given by

$$\boldsymbol{\varepsilon} = \mathbf{L}_w^{\varepsilon} w \tag{1}$$

where

$$\mathbf{L}_w^{\varepsilon} = \begin{cases} -z\begin{bmatrix} \dfrac{\partial^2}{\partial r^2} & \dfrac{\partial^2}{r^2\partial\theta^2}+\dfrac{\partial}{r\partial r} & \dfrac{2\partial^2}{r\partial r\partial\theta}-\dfrac{2\partial}{r^2\partial\theta} \end{bmatrix}^T & \text{for plate} \\ -r\begin{bmatrix} \dfrac{\partial^2}{\partial z^2} & \dfrac{\partial^2}{a^2\partial\theta^2} & \dfrac{2\partial^2}{a\partial z\partial\theta} \end{bmatrix}^T+\begin{bmatrix} 0 & \dfrac{1}{a} & 0 \end{bmatrix}^T & \text{for shell} \end{cases}.$$

While the presented method is formulated for an annular plate and a cylindrical shell, it can be extended to other coordinate frames following a similar procedure of variable separation. For generality, we denote the physical field as $P(t, \mathbf{s})$ in terms of time t and the location vector $\mathbf{s} = [s_1, s_2]^T$ where s_1 and s_2 are two coordinate variables characterizing the mid-surface. In Figs. 1(a, b) or Figs. 1(c, d), (s_1, s_2) represent the (r, θ) or (z, θ) coordinates of an element in the annular plate or cylindrical shell respectively such that ε_{11} and ε_{22} are the normal strains along s_1 and s_2 whereas ε_{12} is the shear strain. Without loss of generality, the time-varying physical field P is expressed as a serial product of time and spatial components:

$$P(t,\mathbf{s}) = \sum_{k=0}^{+\infty} \alpha_k(t)\Phi_k^P(\mathbf{s}) \tag{2}$$

where, Φ_k^P is the k^{th} mode-shape (corresponding to P) determined by the component inertia and stiffness as well as the boundary constraints; and α_k's are the modal coefficients accounting for the accumulative time-varying effects of the intrinsic damping, initial conditions and external inputs. The estimated quantity can be approximated by the modes of the lowest K orders:

$$\tilde{P}(t,\mathbf{s}) = \sum_{k=0}^{K} \alpha_k(t)\Phi_k^P(\mathbf{s}) \tag{3}$$

With measured P at N different locations $\mathbf{s}_j$, $j = 1, 2, \ldots, N$, α_k's can be obtained from (4) according to the least square method:

$$\boldsymbol{\alpha} = (\mathbf{S}^T\mathbf{S})^{-1}\mathbf{S}^T\tilde{\mathbf{P}} \tag{4}$$

where $\tilde{\mathbf{P}} = \left[\tilde{P}(\tau,\mathbf{s}_1)\ \cdots\ \tilde{P}(\tau,\mathbf{s}_N)\right]^T$, $\boldsymbol{\alpha}(t) = \left[\alpha_1\ \alpha_2\ \cdots\ \alpha_K\right]^T$,

and $\mathbf{S} = \begin{bmatrix} \Phi_1^P(\mathbf{s}_1) & \Phi_2^P(\mathbf{s}_1) & \cdots & \Phi_K^P(\mathbf{s}_1) \\ \Phi_1^P(\mathbf{s}_2) & \Phi_2^P(\mathbf{s}_2) & \cdots & \Phi_K^P(\mathbf{s}_2) \\ \vdots & \vdots & \ddots & \vdots \\ \Phi_1^P(\mathbf{s}_N) & \Phi_2^P(\mathbf{s}_N) & \cdots & \Phi_K^P(\mathbf{s}_N) \end{bmatrix}$.

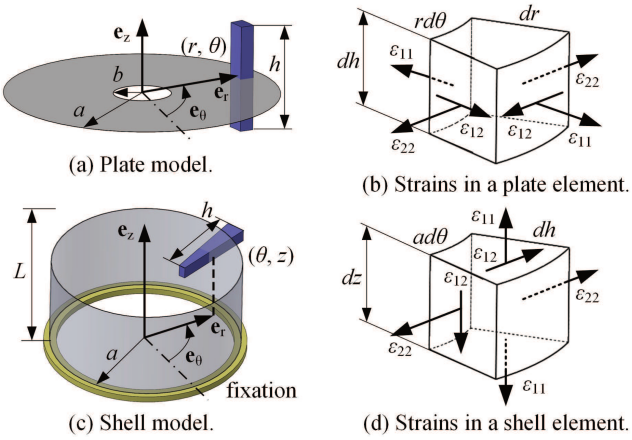

(a) Plate model. (b) Strains in a plate element.

(c) Shell model. (d) Strains in a shell element.

Fig. 1. Models for circular thin-wall components.

A. Field Reconstruction Algorithm

With the general field reconstruction and mode-shapes formulated above, the displacement and strain fields can be independently reconstructed using (2) where the corresponding coefficient $\boldsymbol{\alpha}$ is determined from (4) with corresponding measurements. However, given the displacement and strain fields share the same coefficient $\boldsymbol{\alpha}(t)$ as can be derived from (1), an indirect but simple yet effective approach is employed to determine $\boldsymbol{\alpha}$ from (4) only with measured displacement data. To define dimensionless-variable groups to account for effects of the non-constant thickness on the physical fields

This article has been accepted for publication in a future issue of this journal, but has not been fully edited. Content may change prior to final publication. Citation information: DOI 10.1109/TMECH.2018.2790922, IEEE/ASME Transactions on Mechatronics

$$\frac{e}{\varepsilon}=\frac{1}{h^2/a^2},\quad \frac{W}{w/h}=\frac{R}{r/a}=\frac{\Theta}{\theta}=\frac{Z}{z/L}=1,$$

(1) is rewritten as (5) with the elements (r, θ, z, a) in $\mathbf{L}_w^{\varepsilon}$ replaced with (R, Θ, Z, 1) in $\mathbf{L}_W^e$:

$$\mathbf{e}=\mathbf{L}_W^e W \tag{5}$$

Given that (2) is valid for both displacement and strains, (5) indicates that the normalized strain mode-shapes $\mathbf{\Phi}^e=[\Phi_{11}, \Phi_{22}, \Phi_{12}]^{\mathrm{T}}$ are related to the displacement mode-shape Φ^W via (6):

$$\mathbf{\Phi}^e=\mathbf{L}_W^e\Phi^W \tag{6}$$

Moreover, the modal coefficients $\boldsymbol{\alpha}(t)$ for both displacement and strain fields are identical at each time instance, and $\mathbf{L}_W^e$ is independent of t.

In many applications, non-contact strain measurements are not as accessible as displacement sensing; thus, the indirect approach is employed to reconstruct the strain distributions with the coefficients determined from the displacement measurements using (4) and the procedure is detailed below:

1. Obtain Φ^W for a given configuration from a modal analysis.
2. Differentiate Φ^W to obtain $\mathbf{\Phi}^e$ with (6).
3. Measure w and calculate its normalized value W at the discrete locations $\mathbf{s}_j=\begin{bmatrix}s_1 & s_2\end{bmatrix}_j^{\mathrm{T}}$ where $\mathbf{s}_j=(R_j, \Theta_j)$ or (Z_j, Θ_j), and $j=1, 2, \ldots, N$ across the flexible part surface.
4. Calculate $\boldsymbol{\alpha}$ from (4) where P is specified as W.
5. Obtain the displacement and strain fields by substituting $\boldsymbol{\alpha}$ into (3) with $P=W$ and $P=e$, respectively.
6. Finally, the dimensional quantities w or ε can be obtained from the normalized values.

In Steps 1 and 2 above, the mode-shapes are calculated offline and stored in a database so that the computation does not affect the efficiency of the online reconstruction. The noise due to the derivatives in $\mathbf{L}_W^e$ in (6) can be minimized within a prescribed tolerance using a numerical filter. Unlike commonly used dynamic analysis methods (such as FEA) where $\boldsymbol{\alpha}$ is numerically solved from a large-scale system formulated by the governing differential equations with known inputs, the method introduced here captures the field dynamics with real-time measurements and computes $\boldsymbol{\alpha}$ with simple linear algebraic operations; thus it is practical and efficient for online applications.

B. *Numerical Verification*

The reconstruction method is numerically verified by comparing results with FEA. The annular plate (with a clamped inner-edge and a free outer-edge) is chosen as an illustrative example [23], where the parametric values are listed in Table I; and an impulse response (experimentally captured by an eddy-current displacement sensor) and its frequency spectrum are available in Fig. 2. It is suggested that the plate dynamics can be approximated by the superposition of the lowest three mode-shapes for reconstructing the displacement and strain fields, which justifies the reduction in the number of modes in (3) for subsequent reconstructions. The strain and displacement mode shapes as well as the mode-shape matrix $\mathbf{S}$ of the thin-wall annular plate are numerically calculated using the shooting method [23]. In Table II, the published (1st column) displacement mode-shapes can be used to compute the different strain mode-shapes (2nd to 4th columns) of the lowest orders using (6).

TABLE I. VALUES OF PARAMETERS IN SIMULATION.

Al 1060	**Density ρ**	**Elastic modulus E**	**Poisson υ**
Properties	2.7 g/cm^3	70 GPa	0.35
Dim. (mm)	$a=150$	$b=40$	$h=1$

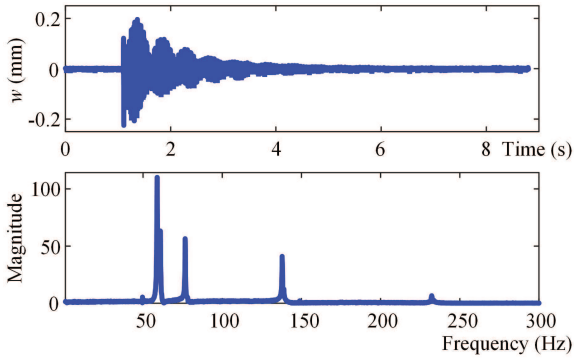

Fig. 2 FFT of vibration measurement [23].

TABLE II. MODE SHAPES.

Mode	Displacement Φ^W [23]	Strains Φ_{RR}	$\Phi_{\Theta\Theta}$	$\Phi_{R\Theta}$
(0, 0)	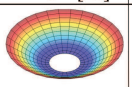	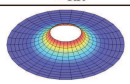	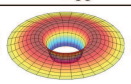	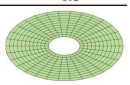
(1, 0)	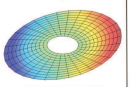	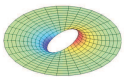	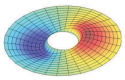	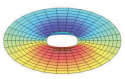
(2, 0)	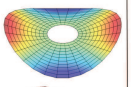	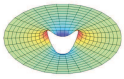	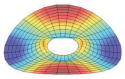	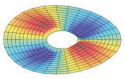
(3, 0)	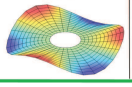	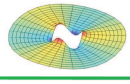	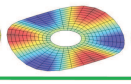	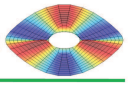

As a basis for verification, the displacement/strain fields of the annular plate are simulated using FEA. The plate is subjected to a normalized concentrated force f_z (= 0.0045, equivalent to 10N for the Al6016 plate) at the free edge (150mm, 0°), and then relieved to simulate a zero-damping free vibration due to a step change. The simulated shape of the plate is shown in Fig. 3(a) where the strains are found primarily in the sector area $-50° \le \theta \le 50°$ around the loading point. Using the FEA results as "simulated measurements", the modal coefficients (α_k where k = 0, 1 and 2) are estimated from (4) using 5 measurements at the cylindrical coordinates r = 110mm and θ = 45°, 315° and at r = 140mm and θ = 0°, 33°, 327°. The static and dynamic (displacement/strain) fields reconstructed from (3) are presented in Figs. 3(c) and 3(d) respectively.

The upper and lower rows in Fig. 3(c) are the static reconstructed fields and their errors relative to the FEA results respectively. The radial strain ε_{rr} (upper row) has its maximum at the fixed inner edge and is zero at the free edge. On the other hand, the tangential strain $\varepsilon_{\theta\theta}$ is zero at the fixed inner edge. Around the loading, $\varepsilon_{\theta\theta}$ is in tensile along two radii and compressive on its bottom surface ($z=-h/2$) which is opposite

This article has been accepted for publication in a future issue of this journal, but has not been fully edited. Content may change prior to final publication. Citation information: DOI 10.1109/TMECH.2018.2790922, IEEE/ASME Transactions on Mechatronics

on the upper surface ($z = h/2$). Unlike the normal (radial ε_{rr} and tangential $\varepsilon_{\theta\theta}$) strains which are symmetric due to bending, the shear strain $\varepsilon_{r\theta}$ is antisymmetric about $\theta = 0°$ because of the plate twisting due to the applied force. The maximum error of the reconstructed strains (after multiplying the normalization factor h^2/a^2) is approximately 10^{-5} where the largest strain is about 10^{-4}. This 10% error (larger than the displacement reconstruction error of approximately 1%) is somewhat expected as the strains are inferred from the measured displacements.

In Fig. 3(d), the reconstructed displacement/strains of the free vibration are compared with the FEA results. The comparisons verify that the proposed reconstruction method can track the time-varying displacement/strains closely when the plate is in free vibration. It is also observed that all the three strains vary with multiple modes like the displacement, validating the formulation of the strain mode-shapes and its field reconstruction application.

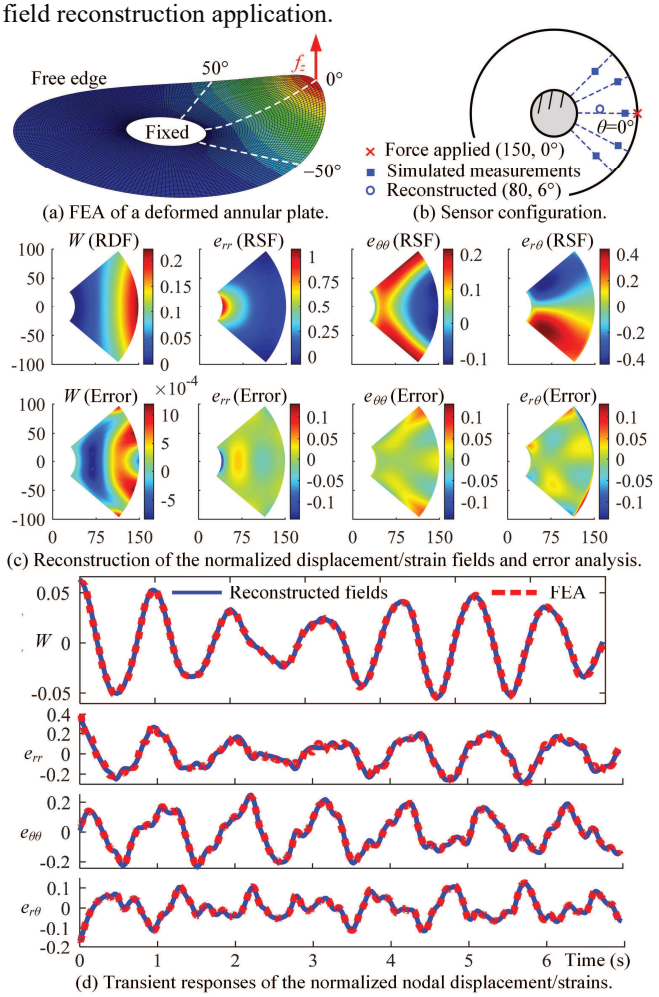

Fig. 3 Field reconstruction verified with FEA.

C. *Numerical Evaluation of Reconstruction Algorithm*

Based on the static analysis, the trade-offs between accuracy and computation time in terms of N sensors and K ($\leq N$) modes are analyzed in Fig. 4: The blue circles in the top plot indicate the % errors of the reconstructed displacement field (relative to the FEA at the maximum value). The red dash-line indicates the upper bound of one standard deviation obtained from 100 tests with up to 10% Gaussian noise added to the simulated measurements to emulate environmental effects on sensed data. The solid-line in the bottom plot represents the time required to calculate one nodal displacement, and the standard deviations (plotted as error bars) are obtained with more than 3500 tests. All the measurements are taken at equally spaced locations along the referenced radius ($\theta = 0°$) of the constraint configuration in Fig. 3(a) with f_z applied at the radius center (95mm, 0°) to represent a general case where a focal force is exerted across the plate. The reconstruction is computed on a desktop computer (Intel i5 CPU 3.3GHz, 8GB RAM); for $N = 5$, it takes about 0.6ms to calculate one reconstruction.

As shown in Fig. 4 (top), the error converges to less than 0.1% with more than five sensors, where the upper bound of the error is limited to 3%. Using the genetic algorithm in the MATLAB Optimization toolbox, the sensing locations are optimized by finding a proper modal coefficient matrix **S** that minimizes the condition number. With the optimized sensing locations, the reconstruction accuracy in Fig. 3 has been significantly improved as compared to that presented in our previous work [29] where the same number of sensors were used. Figure 4 (bottom) shows that the computation time increases linearly with N for $K = N$, and remains almost constant with increasing N for a specified $K = 6$; thus, the computation time required to reconstruct the displacement field is linearly dependent on K. As seen in (4), the reconstruction process involves linear algebraic superposition of K modes implying that more mode shapes for higher reconstruction accuracy would result in a larger modal coefficient matrix and thus longer calculation time. The above conclusions assume that all sensors are distributed equally in space; however, with optimized arrangement of sensor locations, higher reconstruction precision may be obtained with less number of sensors. As the focus here is to develop a reconstruction method, design optimization is briefly described in this work.

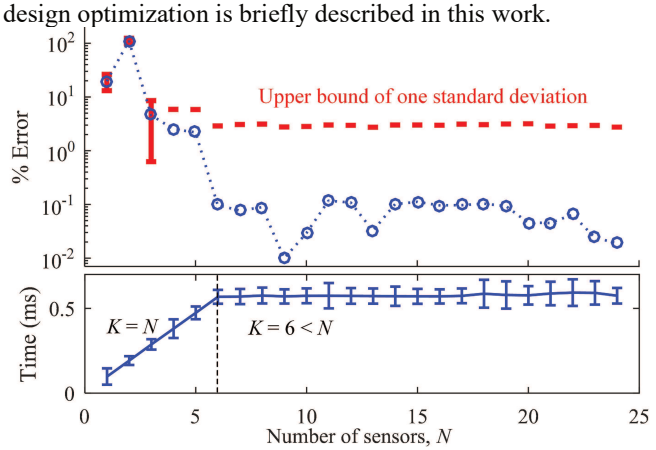

Fig. 4 Reconstruction efficiency.

III. Experiment Results and Illustrative Application

The reconstruction of the displacement and strain fields has been experimentally evaluated on the machining testbed [29]. As shown in Fig. 5(a) where the world referenced frame OXYZ is assigned at the rotation center, the inner portion ($r \leq b$) of a thin-wall plate (Table I) is rigidly mounted on the motor shaft. The machining testbed was modified to allow non-contact

This article has been accepted for publication in a future issue of this journal, but has not been fully edited. Content may change prior to final publication. Citation information: DOI 10.1109/TMECH.2018.2790922, IEEE/ASME Transactions on Mechatronics

measurements on one side of the workpiece (WP) and a displacement-input can be applied on the other side. The fields were reconstructed from a finite number of eddy-current sensors (ESs). To provide an alternative basis for experimental verification, a laser sensor and a pair of strain gauges (SG1 and SG2) were used for measurements of the displacement and strain respectively; however, the latter can only be used in a non-rotating plate experiment. With the sensor specifications detailed in Table III, two experiments were conducted to validate the field reconstruction of the plate subjected to two different inputs; free vibration of a non-rotating plate (Fig. 5b) and lathe machining of a rotating WP (Fig. 5c).

TABLE III. SPECIFICATIONS OF SENSORS.

Eddy-current Sensor (CWY-DO-20XLT08-M10)			
Parameters		**Performance**	
Diameter (mm)	8	Response (kHz)	10
Standoff (mm)	0.5	Range (mm)	2
Input (Vdc)	-24	Resolution (μm)	0.1
Output (Vdc)	–18 to –2	Linearity (±%FS)	1
		Temp. stability (%FSR/°C)	0.04
Laser Displacement Sensor (Keyence LK-H025)			
Parameters		**Performance**	
Ref. distance (mm)	20	Sampling rate (kHz)	2
Spot diameter (μm)	25×1400	Range (mm)	±3
Wavelength (nm)	655	Repeatability (μm)	0.02
Output (mW)	4.8	Linearity (±%FS)	0.02
		Temp. stability (%FSR/°C)	0.01
Strain Gauge (BFH350-1AA-S)			
Parameters		**Performance**	
Gauge pattern	uniaxial	Gauge resistance (Omega)	350
Base diameter (mm)	3.6×3.1	Gauge factor (mV/V)	2±1%
Gauge length (mm)	1.0×2.0	Mechanical hysteresis (μm/m)	1.2
		Range	0.01

A. Free Vibration of Non-rotating Plate

The non-rotating plate (Fig. 5b) was subjected to an initial deflection (w = 0.7mm) specified by a micrometer which was suddenly released to simulate a step displacement-input at (X = 150mm, Y = 0mm). Two mode-shapes (K = 2) of the lowest orders were used for reconstruction from three eddy-current sensors (N = 3) so that the effects of the sensor locations on the reconstruction accuracy can be compared with the published results in [29]. The reconstructed dynamic displacement and strain fields were compared with real-time measurements (w; ε_{rr}, $\varepsilon_{\theta\theta}$) from the laser sensor and uniaxial strain gauges. As shown in Fig. 5(b), the pair of strain gauges was aligned with the circumferential direction and along the radial direction to measure $\varepsilon_{\theta\theta}$ and ε_{rr}, respectively. The test was repeated multiple times with the same initial deflection to allow (ε_{rr}, $\varepsilon_{\theta\theta}$) measurements over a range of angular positions (θ = 0 to 40° in step of 10°). The results are presented in Figs. 6 and 7.

Figure 6 shows that the reconstructed displacement field (RDF) agrees well with the laser measurements, confirming the reconstruction can monitor the plate dynamics featured with multiple modes in real time. It is worth noting that the dominant vibration modes can only be captured by high-speed reconstruction that is generally limited by the sampling rate and calculation time. The sampling rate (2 kHz) employed here is high enough to capture the dominant modes while excluding other higher order modes in the reconstruction considering their negligible vibration amplitudes. With a computation speed faster than 1 kHz (Fig. 4), it is believed that this reconstruction method is sufficiently efficient for a broad range of structural dynamic problems in engineering.

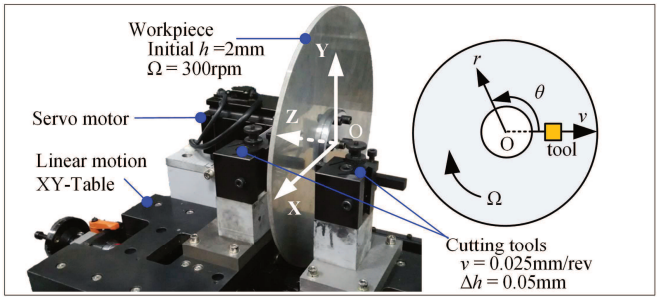

(a) Machining platform.

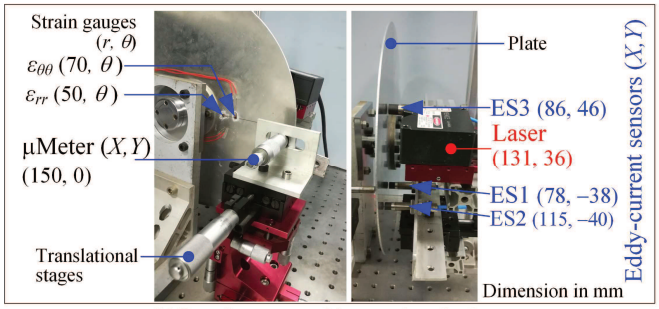

(b) Experiment setup (Non-rotating plate).

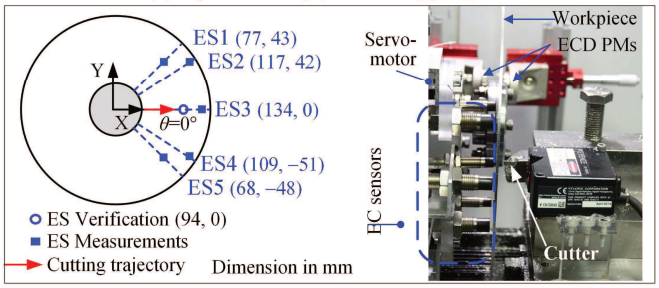

(c) Lathe-machining experimental measurement setup.

Fig. 5 Experiment setups.

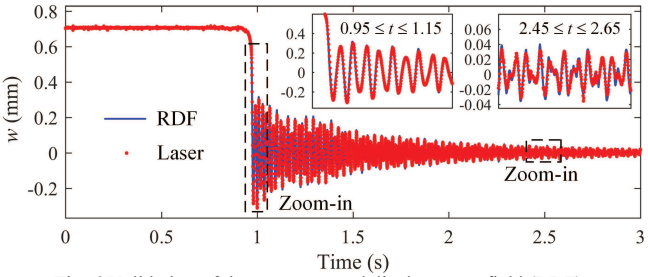

Fig. 6 Validation of the reconstructed displacement field (RDF).

In Figs. 7(a, b), the reconstructed strain (ε_{rr}, $\varepsilon_{\theta\theta}$) fields are compared with the strain gauge measurements, where the error is defined as the difference between the reconstruction and measurement. The % errors are compared in Fig. 7(c) between two reconstructions of the same plate with different sensor locations where (r, θ) are measured in millimeters and degrees respectively:

ES Set 1 (Fig. 6b): (78, –38°), (115, –40°), (86, 46°)

ES Set 2 [29]: (100, –21°), (132, –16°), (106, 28°).

As shown in Fig. 7, all the normal strains respond in a similar fashion as the displacement because their linear relations (1) share the same modal coefficients (4). When θ

This article has been accepted for publication in a future issue of this journal, but has not been fully edited. Content may change prior to final publication. Citation information: DOI 10.1109/TMECH.2018.2790922, IEEE/ASME Transactions on Mechatronics

changes from 40° to 0°, ε_{rr} and $\varepsilon_{\theta\theta}$ increase from 1.2×10^{-4} to 1.9×10^{-4} and from 0.7×10^{-4} to 1.2×10^{-4} respectively while their errors decrease from 2×10^{-5} to about 0.5×10^{-5} (with a lower % error at 0°), which are consistent with the numerical error analysis in Fig. 3(c). The error fluctuation in the static deflection tests was primarily caused by the noise of the strain gauges. The ES Set 1 results in a much smaller % errors than ES Set 2 in the normal strain reconstruction, suggesting that the errors can be reduced by optimizing the ES configuration.

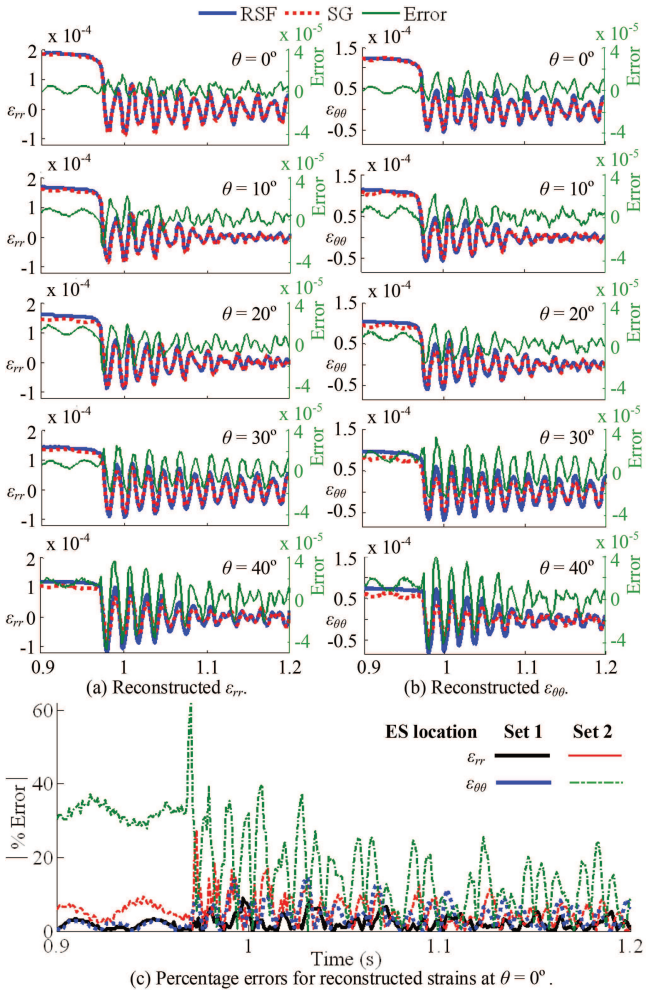

(c) Percentage errors for reconstructed strains at $\theta = 0°$.

Fig. 7 Reconstruction of time-varying strain distributions.

B. *Field Reconstruction for Machining*

An aluminum plate (Table I) was lathe-machined at the rotational speed Ω(= 600rpm) with the depth-of-cut Δh(= 0.05mm) and the tool feedrate v(= 0.0125mm/rev) from the inner edge towards the outer edge as shown in Figs. 5(a) and 5(c) where the pair of permanent magnets (located near the free edge) induces an eddy-current in the plate, which functions as a non-contact eddy-current damper (ECD) to reduce the WP vibration. The fields were reconstructed by superimposing three mode-shapes of the lowest orders (K = 3) from the displacement measurements of five nodal eddy-current sensors (N = 5). The constant depth-of-cut Δh, which is a small fraction (≤ 1/2 [28]) of the plate thickness, has little effects on the mode shapes. The fields were verified with the displacement measured by the 6th ES. Because the surface being machined was oily and partially obscured with chips as the cutter moves outward along θ = 0º, the laser sensor was not used during cutting. The ability to account for the damping effects and external loads in the field reconstruction are demonstrated in Figs. 8 to 10.

Figures 8(a, b) show qualitative comparison of the WP surfaces machined without and with the ECD respectively. The property of the modal coefficients that reflects the dynamic characteristics of the plate is illustrated in Fig. 8(c) where the dominant modal coefficients α_1's of the two cases (without/with ECD) are quantitatively compared. In Fig. 8(c), the thin-dash rectangles indicate the time-intervals (0.15s each) of the zoom-in plots. The low-frequency α_1 variations in both (without/with ECD) cases are primarily due to the WP rotation, whereas the high-frequency variation (in the cutting without ECD) grows from the unstable machining dynamics. As shown in Fig. 8, the time-varying α_1 increasingly fluctuates with the actual depth-of-cut (closely related to the cutting force and WP vibration displacement) as the machined surface changes from smooth to rough during cutting without the ECD. As a comparison, a smaller and persistent variation of α_1 can be seen in the case of cutting with the ECD that effectively dissipates the high-frequency vibration energies yielding a relatively smooth surface.

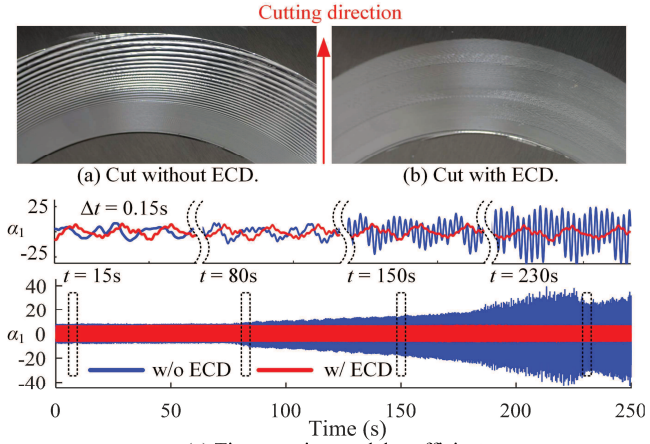

(c) Time-varying modal coefficient.

Fig. 8 Effect of eddy-current damper.

Figures 9(a, b) show the (N = 5) ES measurements and the (K = 3) computed modal coefficients, which provide the basis for the reconstructed displacement and strains at the fixed point (X = 94mm, Y = 0) in the referenced coordinate in Fig. 9(c). As shown in Fig. 9(c), the reconstructed displacement at (X = 94mm, Y = 0) excellently agrees with the ES measurements during machining (forced vibration with non-zero dampings). Figure 10 shows several snapshots of the displacement and strain fields along the timeline over one rotation period in the rotating frame, where the arrow indicates the cutting trajectory for rotation reference. Some observations about the validated field reconstruction in Fig. 10 are highlighted as follows:

– The maximum displacement is located on the opposite side of the cutting area. The most deflected point changing with the rotation period indicates that the intrinsic high-frequency plate dynamics is coupled with the low-frequency rotation, explaining that the low-frequency α_1 variations in Fig. 8(c) are primarily due to the workpiece rotation.

This article has been accepted for publication in a future issue of this journal, but has not been fully edited. Content may change prior to final publication. Citation information: DOI 10.1109/TMECH.2018.2790922, IEEE/ASME Transactions on Mechatronics

– The locations of the respective maximum strain values at each sampling time instance are marked in black and superimposed on the last-column plots. The maximum ε_{rr} occurs at the inner (clamped) edge, and the corresponding location is opposite to the cutting zone.
– The areas for the largest $\varepsilon_{\theta\theta}$ and $\varepsilon_{r\theta}$ are close to the inner edge, specifically about r = 63.1mm. On the other hand, $\varepsilon_{\theta\theta}$ is zero along the clamped edge, and $\varepsilon_{r\theta}$ is zero along the diameter that is being cut.

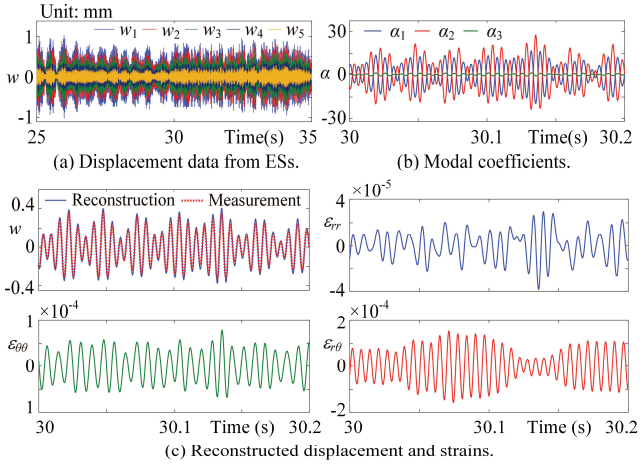

Fig. 9 Reconstruction at (X, Y) = (94mm, 0mm) during machining.

More importantly, the in situ field reconstruction provides a practical real-time feedback of the deflection at the cutting region (Fig. 10) for online compensation of the cutter motions; this relaxes the needs to measure the local WP displacement at the cutting point where stringent space limitations make direct measurements impractical. Additionally, the reconstruction offers a health diagnosis tool that monitors the maximum strains in the WP within its elastic range or its material yielding strain (5×10^{-4} for Al 1060) to prevent built-up of residual strains that is one of the main causes of distortions in final products. As indicated in Fig. 8(c), the modal coefficient potentially plays the role of an alerting signal that monitors the displacement and strains within tolerances. The ability to locate maximum strains facilitates supplemental fixture designs to reduce residual stresses.

IV. Conclusion

A method based on mode superposition has been developed to reconstruct the continuous displacement/strain fields across a flexible workpiece from a finite number of non-contact measurements during machining. This method, which requires no attachment of sensors on the rotating workpiece to reconstruct its strain fields, has been verified numerically and experimentally on a flexible annular plate; both the static deformations and free/forced vibrations are considered. Featured with simple implementation and high efficiency, the reconstruction algorithm takes 0.6ms cycle-time to calculate the displacement/strain fields from five sensors on a desktop computer with a 3.3GHz Intel i5 CPU and 8GB RAM. It is expected that this sensing rate is fast enough to capture the structural dynamics for a broad range of applications. The sensing configuration (both number and location) has been optimized leading to a significantly improved reconstruction accuracy as compared to the previously published results. The method has been evaluated experimentally on a lathe machine testbed, where the dynamics of the distributed physical-field have been successfully captured and analyzed. It is expected that the method presented here will offer an effective basis for developing a health-diagnosis tool for monitoring the maximum strains in the workpiece within its elastic range to prevent built-up of residual strains, which can also be used in real-time feedback for vibration compensation.

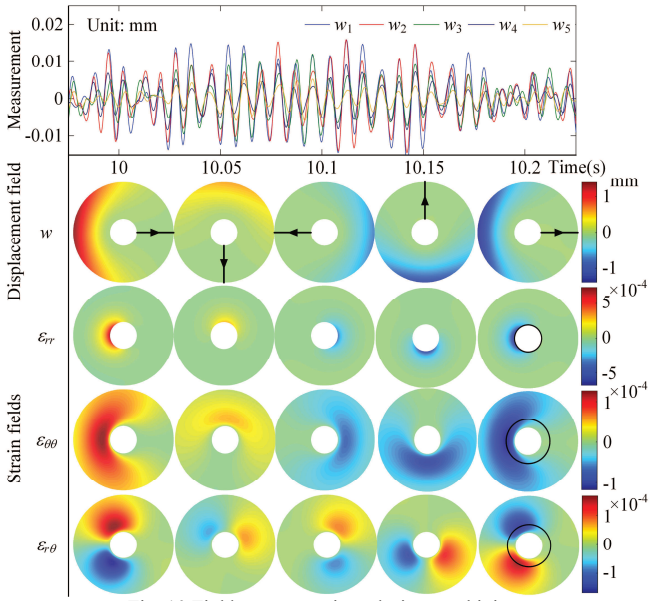

Fig. 10 Field reconstructions during machining.

References

[1] K. Ma, R. Goetz, and S. K. Srivasta, "Modeling of residual stress and machining distortion in aerospace components (preprint)," *Enterprise Soc.*, vol. 9, no. 3, pp. 513-516, 2010.
[2] E. Diez, H. Perez, J. Marquez, and A. Vizan, "Feasibility study of in-process compensation of deformations in flexible milling," *Int. J. Mach. Tool Manu.*, vol. 94, pp. 1-14, 2015.
[3] M. N. Helfrick, C. Niezrecki, P. Avitabile, and T. Schmidt, "3d digital image correlation methods for full-field vibration measurement," *Mech. Syst. Signal Pr.*, vol. 25, no. 3, pp. 917-927, 2011.
[4] D. J. Cappelleri, G. Piazza, and V. Kumar, "A two dimensional vision-based force sensor for microrobotic applications," *Sensor Actuators A Phys.*, vol. 171, no. 2, pp. 340-351, 2011.
[5] M. Y. Tsai, C. W. Ting, C. Y. Huang, and Y. S. Lai, "Determination of residual strains of the emc in pbga during manufacturing and ir solder reflow processes," *Microelectron. Reliab.*, vol. 51, no. 3, pp. 642-648, 2011.
[6] I. Hanhan, E. Durnberg, G. Freihofer, P. Akin, and S. Raghavan, "Portable piezospectroscopy system: Non-contact in-situ stress sensing through high resolution photo-luminescent mapping," *J. Instrum.*, vol. 9, P11005, 2014.
[7] Y. Wang, Y. Li, T. Bock, J. P. Lynch, and J. Mattila, "Introduction to the focused section on intelligent robotics for civil infrastructure," *Int. J. Intell. Robot. Appl.*, vol. 1, no. 3, pp. 239-242, 2017.
[8] B. Li, K. Ushiroda, L. Yang, Q. Song, and J. Xiao, "Wall-climbing robot for non-destructive evaluation using impact-echo and metric learning svm," *Int. J. Intell. Robot. Appl.*, vol. 1, no. 3, pp. 255-270, 2017.
[9] J. Guo, K.-M. Lee, D. Zhu, X. Yi, and Y. Wang, "Large-deformation analysis and experimental validation of a flexure-based mobile sensor node," *IEEE-ASME Trans. Mechatronics*, vol. 17, no. 4, pp. 606-616, 2012.
[10] M. Chierichetti and M. Ruzzene, "Dynamic displacement field reconstruction through a limited set of measurements: Application to plates," *J. Sound Vib.*, vol. 331, no. 21, pp. 4713-4728, 2012.

[11] R. Izamshah, J. P. T. Mo, and S. Ding, "Hybrid deflection prediction on machining thin-wall monolithic aerospace components," *Proc. Inst. Mech. Eng. Part B-J. Eng. Manuf.*, vol. 226, no. B4, pp. 592-605, 2012.

[12] A. Derkevorkian, S. F. Masri, J. Alvarenga, H. Boussalis, J. Bakalyar, and W. L. Richards, "Strain-based deformation shape-estimation algorithm for control and monitoring applications," *AIAA J.*, vol. 51, no. 9, pp. 2231-2240, 2013.

[13] P. Cerracchio, M. Gherlone, and A. Tessler, "Real-time displacement monitoring of a composite stiffened panel subjected to mechanical and thermal loads," *Meccanica*, vol. 50, no. 10, pp. 2487-2496, 2015.

[14] A. Tessler and J. L. Spangler, "A least-squares variational method for full-field reconstruction of elastic deformations in shear-deformable plates and shells," *Comput. Methods Appl Mech. Engrg.*, vol. 194, no. 2, pp. 327-339, 2005.

[15] R. Glaser, V. Caccese, and M. Shahinpoor, "Shape monitoring of a beam structure from measured strain or curvature," *Exp. Mech.*, vol. 52, no. 6, pp. 591-606, 2012.

[16] L. U. Odhner and A. M. Dollar, "The smooth curvature model: An efficient representation of euler-bernoulli flexures as robot joints," *IEEE Trans. Robot.*, vol. 28, no. 4, pp. 761-772, 2012.

[17] R. J. Roesthuis, M. Kemp, J. J. van den Dobbelsteen, and S. Misra, "Three-dimensional needle shape reconstruction using an array of fiber bragg grating sensors," *IEEE-ASME Trans. Mechatronics*, vol. 19, no. 4, pp. 1115-1126, 2014.

[18] S. Laflamme, H. S. Saleem, B. K. Vasan, R. L. Geiger, D. Chen, M. R. Kessler, and K. Rajan, "Soft elastomeric capacitor network for strain sensing over large surfaces," *IEEE-ASME Trans. Mechatronics*, vol. 18, no. 6, pp. 1647-1654, 2013.

[19] J.-W. Park, S.-H. Sim, and H.-J. Jung, "Displacement estimation using multimetric data fusion," *IEEE-ASME Trans. Mechatronics*, vol. 18, no. 6, pp. 1675-1682, 2013.

[20] J. Baqersad, C. Niezrecki, and P. Avitabile, "Extracting full-field dynamic strain on a wind turbine rotor subjected to arbitrary excitations using 3d point tracking and a modal expansion technique," *J. Sound Vib.*, vol. 352, pp. 16-29, 2015.

[21] P. Cerracchio, M. Gherlone, M. Di Sciuva, and A. Tessler, "A novel approach for displacement and stress monitoring of sandwich structures based on the inverse finite element method," *Compos. Struct.*, vol. 127, pp. 69-76, 2015.

[22] Y. Zhao, Y. Zhao, C. Wang, S. Liang, R. Cheng, Y. Qin, P. Wang, Y. Li, X. Li, and T. Hu, "Design and development of a cutting force sensor based on semi-conductive strain gauge," *Sensors Actuators A Phys.*, vol. 237, pp. 119-127, 2016.

[23] J. Guo, K. Lee, W. Liu, and B. Wang, "Design criteria based on modal analysis for vibration sensing of thin-wall plate machining," *IEEE-ASME Trans. Mechatronics*, vol. 20, no. 3, pp. 1406-1417, 2015.

[24] A. A. D. Sarhan and A. Matsubara, "Investigation about the characterization of machine tool spindle stiffness for intelligent cnc end milling," *Robot. Comput.-Integr. Manuf.*, vol. 34, pp. 133-139, 2015.

[25] J. S. Bae, M. K. Kwak, and D. J. Inman, "Vibration suppression of a cantilever beam using eddy current damper," *J. Sound Vib.*, vol. 284, no. 3-5, pp. 805-824, 2005.

[26] J. Laborenz, M. Krack, L. Panning, J. Wallaschek, M. Denk, and P.-A. Masserey, "Eddy current damper for turbine blading: Electromagnetic finite element analysis and measurement results," *J. Eng. Gas Turb. Power*, vol. 134, no. 4, 2012.

[27] J. Guo, R. Liu, and K.-M. Lee, "Displacement field sensing and reconstruction for vibration of a thin-wall plate," presented at the IEEE Int. Conf. on Advanced Intelligent Mechatronics, Busan, Korea, 2015.

[28] J. Guo, R. Liu, and K.-M. Lee, "Dynamic modeling and analysis for thin-wall plate machining," presented at the the ASME Dynamic Systems and Control Conference, Columbus, Ohio, USA, 2015.

[29] M. Yu, J. Guo, and K. M. Lee, "Strain field sensing and reconstruction for a thin-wall plate," presented at the IEEE International Conference on Advanced Intelligent Mechatronics (AIM), Banff, Alberta, Canada, 2016.